# Structural Lines, TINs, and DEMs

James J. Little and Ping Shi
Department of Computer Science
University of British Columbia
Vancouver, BC, Canada, V6T 1Z4
little@cs.ubc.ca 604-822-4830 (Tel) 604-822-5485 (FAX)

Keywords: TIN, DEM, structural lines, constrained Delaunay triangulation, curvature

**Abstract**

*The standard method of building compact triangulated surface approximations to terrain surfaces (TINs) from dense digital elevation models(DEMs) adds points to an initial sparse triangulation or removes points from a dense initial mesh. Instead, we find structural lines to act as the initial skeleton of the triangulation. These lines are based on local curvature of the surface, not on the flow of water. We build TINs from DEMs with points and structural lines. These experiments show that initializing the TIN with structural lines at the correct scale creates a TIN with fewer points given a particular approximation error. Structural lines are especially effective for small numbers of points and correspondingly rougher approximations.*

## 1 Introduction

We begin with dense terrain data specified on a grid of points, a digital elevation model (DEM). From the DEM we derive a triangulation of points selected from the DEM to represent the DEM with minimal error. This triangulation is often called a Triangulated Irregular Network (TIN)[1]. Increasingly these triangulated approximations are used in surface visualization and interaction where the cost of displaying the surface rises with the number of triangles in the representation. Building a triangulation based on an initial skeleton of structural lines representing rapid slope changes reduces the number of points needed to approximate the terrain with a particular error.

The inspiration for this work comes initially from the curve approximation procedure of Douglas and Peucker [2] which derives a polygonal curve that approximates a curve

but recursively finding the farthest point from each segment in the current approximation (Figure 1(a)). In unpublished work, W.R. Franklin (1975) developed a procedure to approximate a terrain height field by iteratively adding the farthest point from each face in a recursively constructed triangulated surface (Figure 1(b)).

Figure 1 around here.

Many techniques for approximating a surface, usually a terrain height field, begin by selecting points that are expected to be critical in the final approximation[3, 4, 5, 6, 7]. The approximation to the surface is improved by adding points to this initial triangulation.

One particular method, [8], finds in each triangle the point that is most poorly fit by the current triangulation and adds that point to the Delaunay triangulation[9] of the points. Iteratively following this process produces triangulations that eventually fit the surface well, but with many fewer points than the source dense data.

It is clear that this method is not guaranteed to fit the surface well at surface discontinuities or at slope discontinuities, both of which occur frequently in terrain and especially in range maps produced in computer vision. The literature[3] abounds with counterexamples. To avoid these failings, Fowler and Little[8] first identify *ridges* and *channels* by simple local geometric operations[10]. Surface water flows away from ridge lines and toward channel lines. These lines are then fit by a polygonal approximation[2] and included in the triangulation by forcing the triangulation to include these lines. Modern methods allow incremental construction of Delaunay triangulation "constrained" by initial line segments[11]. However, any errors in the initial points/lines force the triangulation method to introduce further points, reducing the savings.

Figure 2 around here.

Schmitt and Chen[12] updated Fowler and Little's method by first identifying surface and slope discontinuities and including these lines in the resulting approximation, which uses their own triangulation criterion. They choose lines based on the local differential structure of the surface, which is independent of the choice of coordinate system and is not necessarily coincident with the paths determined by the flow of water[13]. [14, 15] also insert "crest" lines into adaptive meshes to improve stereo-driven surface approximation. The resulting lines are not necessary ridges or channels, rather local extrema of curvature (coordinate system independent). We refer to lines where the local curvature is positive as *p-lines* and to lines of negative curvature as *n-lines*. These comprise the *structural lines* of the surface. The p-lines for a section of the Crater Lake, Oregon, USGS 1:24000 DEM (Fig. 2(a)) are

shown in white in Fig. 3, both at medium scale (a) and fine scale (b). The scale of the DEM is the amount of Gaussian smoothing that has been applied. There are ridges and channels that do not coincide with structural lines; slope breaks are structural lines that do not mark ridges or channels. The method of deriving these p-lines and our notion of scale will be explained in Section 2.

Figure 3 around here.

The significance of surface lines is related to their role in the surface representation. Building a triangulation based on an initial skeleton of structural lines reduces the number of points needed to approximate the terrain with a particular error. For hilly terrain (Crater) including structural lines reduced the size of the TIN by as much as 31%; for smoothly varying terrain (Yakima), the reduction is as much as 48%. Using structural lines always reduces the size of the triangulation.

We will first describe how to derive structural lines from local curvature descriptions. Then we will show how these lines are used in the Constrained Delaunay Triangulation of the surface, and how to adjust the position of lines found at coarser scales to the correct position at fine scales. Finally we will present experiments using structural lines in TINs, showing how smoothing selects the important lines, and how correcting position improves the compactness of the triangulation.

## 2 Curvature Descriptions

Figure 4 around here.

In [8], ridges are found by marking the points to which water would flow[10], leaving unmarked the ridge lines (see Fig. 4(a)). The channels are found by marking points from which water would flow. Even this method finds many small segments of little importance. Steger [16] finds watersheds on a smoothed surface by following the gradient direction from saddle points.

Because of quantization and noise, it is important to filter the surface by smoothing with a Gaussian filter whose scale is described by the parameter $\sigma$. We compute derivatives with regard to an underlying continuous surface that has been sampled and quantized. Estimating derivatives is ill-posed [17], that is, it is unstable in the presence of noise; quantization itself introduces noise. Gaussian smoothing regularizes the derivative computation, reducing the instability. Effectively this smoothing, on regularly sampled data, fits a spline to the surface whose scale is determined by $\sigma$. Derivatives computed on the smoothed surface vary continuously and the gradient direction is not restricted to the raster directions.

Figure 4(b)) shows the ridge lines after the DEM has been smoothed by a Gaussian filter with $\sigma = 2.5$ to reduce quantization effects. Despite the smoothing, the ridge lines are interrupted by many gaps.

Instead of marking ridges and channels, we determine local surface properties independent of the coordinate system. We find surface structural lines perpendicular to which surface slope changes sharply; these include most ridges and channels, as well as slope breaks. Like [14, 15, 18, 19], we determine the local surface curvature description.

Figure 3 shows the effect of smoothing with different scales—at the coarser scale the curves are better connected and some small curves have been eliminated. When computing curvature the scale at which the features are computed matters; the scale refers to the amount of simplification or smoothing of the surface when curvature is computed. Smoothing eliminates small surface perturbations (Fig. 5).

Figure 5 around here.

At each point the tangent plane is computed; it is orthogonal to the surface normal $\vec{n}$. The surface can be cut by a plane containing $\vec{n}$. Each such plane defines a direction $\vec{v}$ in the tangent plane; the the *normal* curvature in the direction $\vec{v}$ is the curvature of the curve formed by the intersection of the surface and the plane. The *principal directions* are the two orthogonal directions $\vec{t_1}$ and $\vec{t_2}$ where the value of the normal curvature reaches its maximum and minimum values, $k_1$ and $k_2$. We choose subscripts so that $k_1$ is the curvature of maximum absolute value and $\vec{t_1}$ and $\vec{t_2}$ are vectors in the local tangent plane pointing the direction of maximum and minimum curvature.

To compute these quantities, we first locally determine the surface derivatives and from them the first and second fundamental forms. The curvature and the principal directions are then computed(see [20]). The principal directions on the surface define a net[21]. At a slope break, $k_1$ will be large and $k_2$ will be small. The surface along such slope break lines will be approximately cylindrical. Figure 6(a) shows a surface with the local geometrical structure.

Figure 6 around here.

To find structural lines we determine whether the maximum curvature $k_1$ at each point is locally maximal in the principal direction $\vec{t_1}$. Figure 6(b) shows the structural lines for a surface with sinusoidal cross section. Figure 7(a) shows the height image of a paraboloid; its cross section is an inverted parabola. The image of $|k_1|$ for the paraboloid appears in (b). The rightmost image shows the points of maximal curvature in direction $\vec{t_1}$.

Figure 7 around here.

Figure 8 around here.

The image of $|k_1|$ for Crater Lake appears in Fig. 8(a); higher values appear darker. We use non-maximum suppression to identify these points; we look in the direction of maximum curvature, $\vec{t_1}$, and mark points where $|k_1|$ is greater than neighboring points along the line of curvature in that direction, both forward and backward. The result of non-maximum suppression is a set of points forming curves, each labeled with $|k_1|$ (Fig. 9).

Figure 9 around here.

A *p-line* is a line connecting points of locally maximal positive curvature. An *n-line* is such a line with negative curvature. To find these lines, we track lines and connect the points, employing hysteresis with thresholding, using the magnitude of the maximum curvature[22]. The parameters $low$, $high$, $minlength$ are based on the distribution of curvature magnitude. Once the points of maximal curvature are linked into curves, points below $low$ are eliminated. Points above $high$ are kept; points between between $low$ and $high$ are kept if they are connected to a point above $high$ by points above $low$. Connected sets of points are pruned if shorter that $minlength$ points. Tracking, followed by pruning short lines, produces the p-lines and n-lines shown in Fig. 3; several scales are superimposed in Fig. 11(a). Eliminating short lines aids in selecting the scale of surface feature that can be represented by the structural lines.

Compare the p-lines in Fig. 14(a) in black at scale $\sigma = 4.0$ to the p-lines (white) in Fig. 3(a) at scale $\sigma = 2.5$ and to the p-lines (white) in Fig. 3(b) at scale $\sigma = 1.0$. As $\sigma$ increases the number of p-lines decreases. As experiments in Section 4 show, smoothing eliminates creases unimportant to the final triangulation. Here we deal with three scales: coarse $\sigma = 4.0$, medium $\sigma = 2.5$, and fine $\sigma = 1.0$.

Figure 11 around here.

Most of the structural lines coincide with ridges and channels, i.e., where $t_2$, the principal direction along the structural line, is parallel to the gradient $(dx, dy)$. In Fig. 9(a), approximately 16.8% of the p-lines at medium scale (2.5) are slope breaks that do not satisfy this condition.

## 3 Triangulation

In the original work in this area[8], two innovations were proposed: incremental "greedy" triangulation of a TIN by inserting points based upon the error in each triangle, and preservation of structural lines found by marking p-lines and n-lines and then generalizing these 3D lines. Incremental improvement is widely used now, together with many variations in criteria for adding points. We include in each triangle the point (the "worst" point) with most error in the current approximation.

Many different strategies can be used for determining the order of insertion. [8] proceeded by inserting the worst point in a triangle if it exceeded a desired error tolerance, continuing until all points in the DEM were fit within this tolerance by the triangulation.

[3] introduced the idea of "batching" updates. In each triangle, they find the point worst fit by some criterion, usually the vertical error; these points are the *candidate* points. Then they only insert those candidate points whose error exceeds some fraction $\alpha$ of the current maximum error. In our algorithm, we sort all candidate points and only insert the top $\alpha$ percent of these points at each pass. $\alpha$ is set at 1 in our experiments. Let $n$ be the number of points in the DEM, $N$ the desired number of points in the triangulation, and $I$ the number of points in the initial skeleton. We define $\beta$ as the ratio of points in the triangulation after one pass of greedy insertion to the number in the previous triangulation. There is one candidate point per triangle, whose number is bounded above by twice the number of points in the current triangulation. Thus $\beta$ will be approximately $1 + 2\alpha$; for us this is 1.02. The number of iterations $K$ is then determined by

$$N = (\beta)^K \, I,$$

and therefore

$$K = \frac{\log(N/I)}{\log \beta}.$$

For example, our Crater Lake TIN begins with a skeleton of $I = 496$ points, finishing with $N = 5000$ points; $K$ is then estimated as 116.8. In practice there are $K = 119$ iterations. $N$ is usually set at some fraction on $n$, so the number of iterations is proportional to $\log n$.

At each iteration all points in new triangles must be examined. After iteration $i$ there are $N_i$ points and approximately $\beta N_i$ new triangles to test. There are, on average, $n/N_i$ DEM points per triangle at iteration $i$. The expected number of DEM points that must be examined is then $\beta n$, at every iteration, which is $O(n)$.

Inserting a point in a CDT is $O(\log n)$. Each of $K$ steps then costs $O(n \log n)$, and therefore the total cost is $O(n \log^2 n)$. In practice the triangles to be examined (bounded by number of points inserted) could be stored in a list, and candidate points stored in a

priority queue. This would would not change the complexity, since $O(n)$ DEM points must be examined, but would bring significant practical speedup.

The second innovation of [8] is not often used since finding structural lines is complex. Fowler and Little forced the structural lines into the triangulation after inserting points. Since that time, Constrained Delaunay Triangulation (CDT) has become well understood so structural lines will be inserted initially as part of the triangulation. We have the adapted the incremental CDT software of Dani Lischinski (`http://www.cs.huji.ac.il/ danix/`) to insert points based on the error between the current triangulation and the DEM.

### 3.1 Snakes: Deforming Coarse Scale Lines

Lines found at the medium scale ($\sigma = 2.5$) may have been displaced by the smoothing process. Smoothing an asymmetrical hill, where slope on one side is significantly steeper than the other, will displace the maximum (where the p-line lies) toward the the less steep side (Fig. 10). When structural lines found after smoothing form the skeleton of the surface, the triangulation process must include "corrective" points near the p-line to model the actual location of the crest, increasing unnecessarily the size of the triangulation.

Figure 10 around here.

To move the lines from the smoothed surface to the location of the fine-level line, we use the "snake" method[23, 24, 25]. The essential idea of snakes is to deform the initial line until it reaches a new position close to the line at the fine scale. The snake method deforms the line to minimize the sum of "internal energy", the energy of stretching the line, and "external energy", the energy from the attractive force applied by some external source, in this case a field derived from the lines at the finer scale. The proximity field for the fine scale p-lines in Crater Lake appears in Fig. 8(b). We use the actual curvature field computed at the finer scale (Fig. 8(a)) instead of proximity; the external energy at a point is $-|k_1|$.

Deforming the lines is an iterative process; at each step, each point checks neighboring points and finds the location that minimizes its local energy. Local solutions are combined using dynamic programming; we have used the implementation described in [24]. Each iteration reduces the energy of the curve being deformed and requires $O(n)$ computation. In our experiments the number of iterations per curve was approximately 5. Figure 12 shows the medium scale lines (black) and the snaked result (white) superimposed on the local maximum curvature field.

Figure 12 around here.

Several options and issues arise:

- retraction
  In a snake the external force field attracts the curves and the stretching of links between points generates energy as the curve deforms to fit external forces. In an open curve, (Figure 13) the curve will retract toward local maxima; the retraction does not retract the lines further. The curve can reduce energy by moving the end point along the line even if there is an adjacent point; there is no energy increase on compression. An endpoint at position 0 will move to position 1 only if the reduction in energy from external forces $dE = (E_1 - E_0) - K$ is negative; $dE < 0$ means the point will move. $E_i$ is the external energy at position $i$. $K$ is a coefficient balancing external and internal forces; $-K$ represent the reduction in stretching energy from moving one unit. It is set at approximately the average value of gradient of external force, which is scaled to 255. $K$ is usually set at 10. If the end of the line lies near a relative maximum of attractive force, the endpoint will move toward the maximum, along the line, thus shrinking the line. Reducing $K$ to 0 is not a solution, since the snaked line then wiggles to adjust to small local variations in the curvature field.

- using absolute value of maximum curvature or proximity
  The maximum curvature field moves coarser scale lines along the gradient of maximum curvature. The proximity field (Fig. 8(b)) does not vary in strength along the line, only away from it. The proximity field does not contain any shape information, only the spatial location of the fine scale line. In fact, retraction might increase, since points may move along the fine scale line.

Retraction of lines in Fig. 11(b) reduced the total number of curve points by 28%. The snake process only considers lines of a certain minimum length; this imposes a scaled constraint based on spatial extent in the input data. Retraction appears to be a benefit since it removes the tails of lines extending into areas that are not significant at fine scale. These effects are discussed in the next section.

Figure 13 around here.

# 4 Experiments

To determine whether including structural lines can improve triangulation, we compare triangulations produced by pure "greedy" triangulation, with no lines (called no lines), with "greedy" constrained Delaunay triangulation (CDT) with a variety of structural lines.

The various structural lines are:

- curvature-based structural lines at fine scale (fine, $\sigma = 1.0$)
- curvature-based structural lines at medium scale (medium, $\sigma = 2.5$)
- curvature-based structural lines at coarse scale (coarse, $\sigma = 4.0$)
- medium scale structural lines corrected to a fine scale (snaked)
- coarse scale structural lines corrected to a fine scale (csnaked)

The curvature-based structural p-lines are shown in Fig. 11(a), in white, for the fine scale (used in fine). The medium scale p-lines (medium) are shown in black in both parts of the figure; in Fig. 11(b), they appear, in white, corrected to fine scale using the snake method of Sec. 3.1. These are used in snaked.

Figure 14 around here.

The full process of deriving structural lines is:

1. smooth the DEM with a Gaussian filter (parameter $\sigma$)
2. derive curvature-based lines by computing the absolute value of the maximum curvature (Fig. 8(a)), then find locally maximal points (Fig. 9)
3. link the locally maximal points into curves, using thresholding with hysteresis (parameters $low$, $high$, $minlength$) (Fig. 11(a)). $high$ is set to select a certain percentage of points in the DEM. $low$ is set to 1.
4. snake the curves to fine scale, (parameters $K$ and $minlength$) (Fig. 11(b))
5. simplify the curves in 3D using the Douglas-Peucker method (parameter $gen$) (Fig. 14)

The time and space complexity of steps one through four are $O(n)$, where $n$ is the number of pixels in the image. These processes reduce the number of points in the snaked lines to approximately 5% of $n$. Step five, curve simplification, is $O(n^2)$. Despite this, all five steps take approximately the same amount of time.

[26] describes how to determine the region surrounding a p-line (or n-line) and then compute a surface measure that can be integrated over the region or along the line, including, for example, area, surface area, or slope. Figure 15 shows the connected regions of positive maximum curvature surrounding p-lines in the central region of the Crater Lake DEM. A scalar measure of the line or region provides a metric criterion for preferring some structural lines over others. Structural lines for small surface creases contribute little to the overall surface structure and need not be included in the initial skeleton.

Figure 15 around here.

Experiments in producing TINs were run on the Crater Lake DEM, running the batched greedy triangulation (subject to constraints provided by structural lines) and inserting only the top $\alpha = 1$ percent of the candidate points. The DEM contains 154224 points, ranging in height from 1533 to 2478, a height difference of 945. The triangulation stopped when 5000 points, or 3% of the original points, had been included.

Figure 16 around here.

Figure 17 around here.

To understand the effect of using structural lines in the triangulation, we plot the number of points required as a function of the root-mean-square error (RMSE) in Fig. 16. The RMSE is computed as $\sqrt{\frac{\sum_{i=1}^{n} e_i^2}{n}}$ at all DEM points $i$. $e_i$ is the difference between the DEM height at $i$ and the TIN approximation. Fewer points proportionally are required when the approximation error is large (Fig. 17). The mean-absolute error (MAE) is computed at points $i$ in the DEM as $\frac{\sum_{i=1}^{n} |e_i|}{n}$. The MAE is less sensitive to large errors than the RMSE and gives a better picture of the behavior of the approximation.

In all cases the results using csnaked, the lines from a coarse scale corrected to a fine scale by snakes, were superior. The results can be presented in a tabular form. For RMSE, MAE and MAX (maximum vertical error over the entire TIN), it is clear that the csnaked TIN uses fewer points than the TIN produced with points alone. Table 2 shows the average ratio of the number of points in the triangulation produced using each type of structural line to the number of points in a triangulation with no lines, for various RMSE, MAE and MAX values. The ranges are, first, a broad set of values, then the error range for fine approximations, and then for rough approximations. The number of points in the TIN varies from from 0.43% of the DEM for rough approximations to 3.1% for fine.

Figure 18 shows the triangulations produced by the two methods; the constrained lines are shown in black and other edges in white. Triangulation (a), without lines, uses 700 points to achieve a fit whose RMSE is 12.5, while the triangulation using structural lines (b) has the same RMSE with only 556 points, 21% fewer points. The points are more evenly spread through the DEM in (b), and it may seem that the improved triangulation results from the better set of initial points. However, the edges are important: including only the points in csnaked yields an 8-12% reduction instead of 16-23%.

In summary, all structural lines are better than not including lines; csnaked is best, using, over a broad range, 16% points fewer for RMSE, 21% fewer for MAE, and 34% for MAX. For rougher approximations (few points and less accuracy), csnaked used 23% fewer for RMSE, and 31% fewer for MAE. The results using lines for maximum error (MAX) are

better for fine approximations, where lines reduces the number of points needed by as much as 44%.

Table 1 around here.

Further experiments tested the benefits of structural lines on terrain regions with large essentially flat areas, drawn from a section of the USGS 1:24000 DEM for Yakima, Washington, shown in Fig. 2(b). The Yakima DEM contains 65536 points, ranging in height from 245 to 853, a height difference of 608. As before, we graph the number of points required as a function of RMSE in Fig. 19. Again, fewer points proportionally are required when the approximation error is large (Fig. 20).

Figure 19 around here.

Figure 20 around here.

The results in the Yakima DEM are even better than the results for the Crater Lake DEM (Table 1). snaked is best, using 23% points fewer for RMSE and 44% fewer for MAE over a broad range. The point range is similar to the Crater samples. For rougher approximations (few points and less accuracy), it used 23% fewer for RMSE and 48% fewer for MAE. In this DEM, using structural lines does not reduce the MAX error. For a similar DEM near Tucson, structural lines reduced the MAX error by 19% for fine approximations.

Table 2 around here.

Two issues arose in the discussion of snaking: retraction and attractive forces. We suggested that line retraction during snaking was beneficial. The snake process can be controled so that lines do not retract along their length. The results are mixed: for fine approximations the preserved (without retraction) lines are slight improvements. For rougher approximations, they are significantly worse.

We also considered using the proximity field (Fig. 8(b)) instead of maximum curvature field (Fig. 8(a)) for snaking; for the Crater the results using proximity are 3.6% reduction versus 12.6% for similar parameters using the maximum curvature field.

Each DEM has its own proper scale: csnaked at $\sigma = 4.0$ is best for Crater Lake, while snaked at 2.5 is best for Yakima. Crater Lake has average gradient magnitude 5.00 and maximum 148.66 while Yakima has average gradient magnitude 3.79 and maximum 71.11. Smoothing selects the spatial scale of the structural lines and should vary with the DEM.

## 5 Discussion

How have we advanced beyond the work of Fowler and Little[8]? We have a sounder basis for local surface description; our method is more immune to quantization introduced in the DEM, and is not coordinate system dependent. It permits description of all surface breaks, not just those that coincide with ridges and channels.

The inclusion of lines in the construction of TINs reduces the number of points required to achieve a particular accuracy of approximation, measured either by RMSE or MAE. Alternatively, at a particular size of the TIN, the accuracy achieved is greater when structural lines are included.

Finding curvatures requires estimating derivatives. Smoothing or regularization reduces the effects of noise in computing derivatives but this impedes localization. The snake method lets us extract significant lines at coarser scales and correct them to improve their localization for use in the TIN. Methods such as anisotropic diffusion[27] that would combine smoothing and localization may aid determination of structural lines.

Edge focusing[28] suggests finding edges at fine scale from coarser scales by tracking the edges, searching at the next finer scale for edges. They are shown to move, under reasonable assumptions, only a small amount. Our snaking has been from coarser scales directly to fine scale ($\sigma = 1.0$). As an alternative we could proceed by gradually snaking using intermediate values of $\sigma$. Retraction during snaking makes this complex, requiring further insight into both the movement of structural lines as the surface is smoothed and the behavior of snakes.

If p-lines at coarser scales happen to lie near n-lines at fine scale deforming all curves at the same time might move the p-line incorrectly towards the n-line. The maximum curvature field can be separated into positive and negative terms and p-lines and n-lines treated separately. We have left further work into this area until later.

For hilly terrain such as Crater Lake structural lines reduced the size of the TIN by as much as 31%; for smoothly varying terrain such as the Yakima region, the reduction is as much as 48%. Other similar regions such as a DEM of Mt. Baker, Washington, achieved similar results to Crater Lake; its MAE for a coarse approximation was 30% smaller than without lines. A DEM near Tucson behaved like Yakima, having a MAE reduction of 44%. Using structural lines always improves the triangulation.

There are many alternative methods for choosing the best point for insertion and for adjusting the resulting triangulation (see, e.g., [29, 4, 30, 31]) but we have not explored these here. Some may perform much better when structural lines are used. The usual criterion for quality of approximation is the root-mean-square of the error, but this does not capture the importance of the structural lines such as ridge lines, streams, and slope

breaks. In many visualization tasks, however, retaining features such as horizon lines is more important than aggregate errors. In drainage queries[32] and other such applications, preserving the structural lines is critical.

## References


[1] T. K. Peucker, R. J. Fowler, J. J. Little, and D. M. Mark. The Triangulated Irregular Network. In *Proc. of the Digital Terrain Models Symp.*, pages 516–532, St. Louis, MO, 1978.

[2] David H. Douglas and Thomas K. Peucker. Algorithms for the reduction of the number of points required to represent a digitized line or its caricature. *The Canadian Cartographer*, 10(2):112–122, 1973.

[3] Michael Garland and Paul S. Heckbert. Fast polygonal approximation of terrains and height fields. Technical Report CMU-CS-95-181, Carnegie Mellon U., September 1995.

[4] M.F. Polis and D.M. McKeown. Iterative TIN generation from digital elevation models. In *Proc. IEEE Conf. Computer Vision and Pattern Recognition, 1992*, pages 787–790, 1992.

[5] Paul S. Heckbert and Michael Garland. Survey of polygonal simplification algorithms. Technical report, CMU, 1997.

[6] Mark P. Kumler. An intensive comparison of triangulated irregular networks (TINs) and digital elevation models (DEMs). *Cartographica*, 31(2):1–48, 1994.

[7] Martin Heller. Triangulation algorithms for adaptive terrain modeling. In *Proceedings of the 4th International Symposium of Spatial Data Handling*, pages 163–174, 1990.

[8] Robert J. Fowler and James J. Little. An automatic method for the construction of irregular network digital terrain models. In *Proceedings of SIGGRAPH '79*, pages 199–207, Chicago, Illinois, August 1979.

[9] Dani Lischinski. Incremental Delaunay triangulation. In P. Heckbert, editor, *Graphics Gems IV*. Academic Press, 1994.

[10] T.K. Peucker and D.H. Douglas. Detection of surface-specific points by local parallel processing of discrete terrain elevation data. *Computer Graphics and Image Processing*, 4:375–387, 1975.

[11] D. G. Kirkpatrick. Efficient computation of continuous skeletons. In *Proc. of the 20th Annual IEEE Symposium on Foundations of Computer Science*, 1979.

[12] Francis Schmitt and Xin Chen. Vision-based construction of CAD models from range images. In *Proc. 4th International Conference on Computer Vision*, pages 129–136, 1993.

[13] J.J. Koenderink and Andrea van Doorn. Local features of smooth shapes: Ridges and courses. In *SPIE(2031)*, pages 2–13, 1993.

[14] Richard Lengagne, Oliver Monga, and Pascal Fua. Using differential constraints to reconstruct complex surfaces from stereo. In *Proc. IEEE Conf. Computer Vision and Pattern Recognition, 1997*, pages 1081–1086, 1997.

[15] Pascal Fua. Model-based approach to accurate and consistent 3-D modeling of drainage and surrounding terrain. In *Proc. IEEE Conf. Computer Vision and Pattern Recognition, 1997*, pages 903–908, 1997.

[16] Carsten Steger. Subpixel-precise extraction of watersheds. In *ICCV-99*, pages 884–890, 1999.

[17] T. Poggio, V. Torre, and C. Koch. Computational vision and regularization theory. *Nature*, 317:314–319, 1985.

[18] O. Monga and S. Benayoun. Using partial derivatives of 3D images to extract typical surface-features. *Computer Vision Graphics and Image Processing: Image Understanding*, 61(2):171–189, March 1995.

[19] Joseph Wood. Modelling the continuity of surface form using digital elevation models. In *International Symposium on Spatial Data Handling '98*, pages 725–736, June 1998.

[20] O. Faugeras. *Three-Dimensional Computer Vision*. MIT Press, Cambridge, MA, 1993.

[21] J. J. Koenderink. *Solid Shape*. MIT Press, Cambridge, MA, 1990.

[22] J. F. Canny. A computational approach to edge detection. *IEEE Transactions on Pattern Analysis and Machine Intelligence*, 8(6):679–698, 1986.

[23] M. Kass, A. Witkin, and D. Terzopoulos. Snakes: Active contour models. *International Journal of Computer Vision*, 1:321–331, 1988.

[24] A.A. Amini, T.E. Weymouth, and R.J. Jain. Using dynamic programming for solving variational problems in vision. *IEEE Transactions on Pattern Analysis and Machine Intelligence*, 12(9):855–867, September 1990.

[25] S. Chandran, T. Maejima, and S. Miyazaki. Global minima via dynamic programming: Energy minimizing active contours. In *SPIE Vol 1570, Geometric Methods in Computer Vision*, pages 391–402, 1991.

[26] James J. Little and Ping Shi. Structural lines for triangulations of terrain. IEEE Workshop on Applications of Computer Vision, 1998.

[27] Marc Proesmans, Eric Pauwels, and Luc van Gool. Coupled geometry-driven diffusion equations for low-level vision. In *Geometry-Driven Diffusion in Computer Vision*, chapter 7, pages 191–227. Kluwer Academic, 1994.

[28] F. Bergholm. Edge focusing. *IEEE Transactions on Pattern Analysis and Machine Intelligence*, 9:726–741, 1987.

[29] Zi-Tan Chen and J. Armando Guevara. Systematic selection of very important points (VIP) from digital terrain model for constructing triangular irregular networks. In N. Chrisman, editor, *Proc. of Auto-Carto 8 (Eighth Intl. Symp. on Computer-Assisted Cartography)*, pages 50–56, Baltimore, MD, 1987. American Congress of Surveying and Mapping.

[30] Nira Dyn and Shmuel Rippa. Data-dependent triangulations for scattered data interpolation and finite element approximation. *Applied Numer. Math.*, 12:89–105, 1993.

[31] Bernd Junger and Jack Snoeyink. Importance measures for TIN simplification by parallel decimation. In *International Symposium on Spatial Data Handling '98*, pages 637–646, 1998.

[32] Sidi Yu, Marc van Kreveld, and Jack Snoeyink. Drainage queries in TINs: From local to global and back again. In *7th Symp Spatial Data Handling*, pages 13A.1–13A.14, 1996.

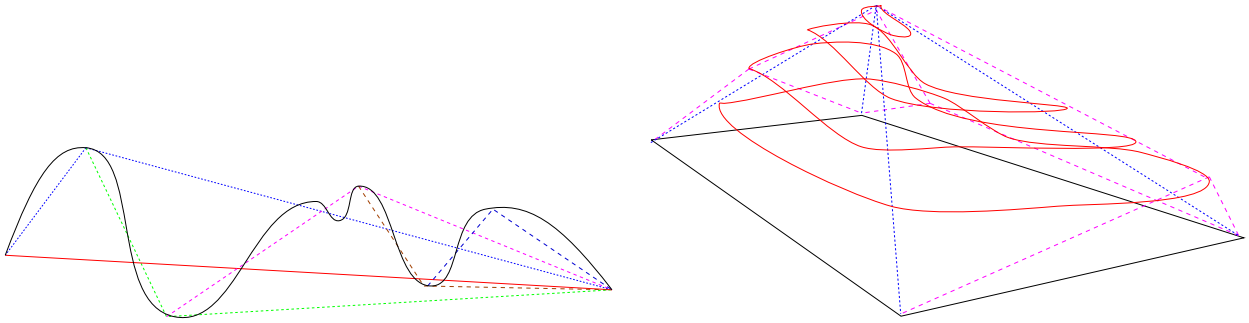

(a) (b)

Figure 1: (a) Curve simplification: the Douglas-Peucker method adds the farthest point from each segment on the current polygonal curve. Successive approximations are show by progressively finer dashed lines. (b) Terrain surface represented by contours: as before, successive approximations are shown with progressively finer dashed lines.

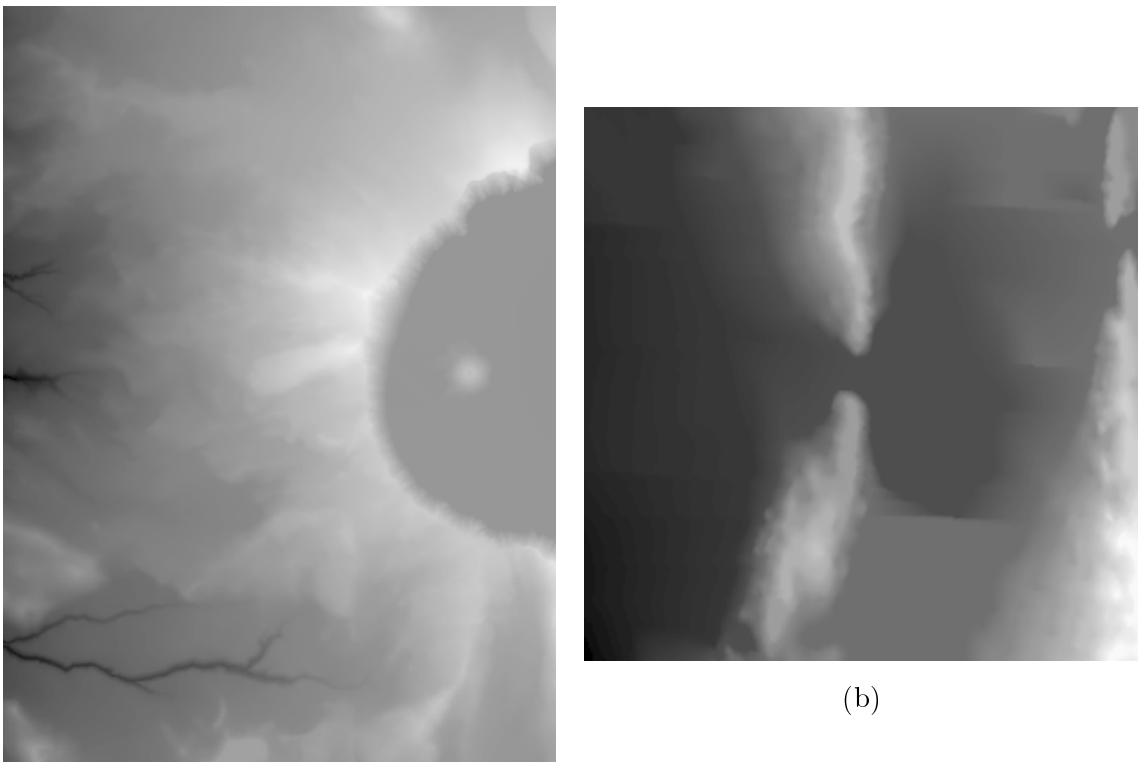

(a) (b)

Figure 2: DEMs for (a) Crater Lake (b) Yakima. Both show gray value proportional to elevation.

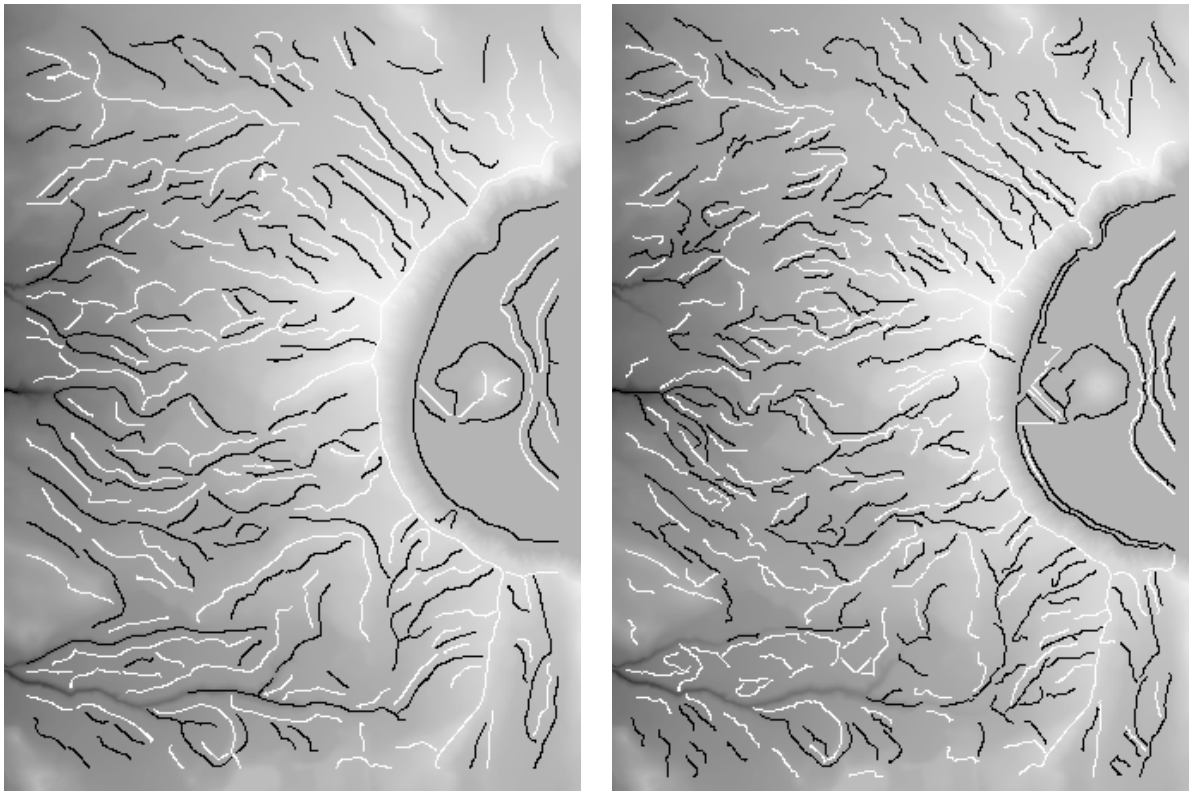

(a) (b)

Figure 3: (a) p-lines (white) and n-lines (black) at medium scale ($\sigma = 2.5$) overlaid on the Crater Lake DEM; (b) p-lines and n-lines ($\sigma = 1.0$). $\sigma$ is the scale parameter of a Gaussian filter that smooths the DEM before computing structural lines.

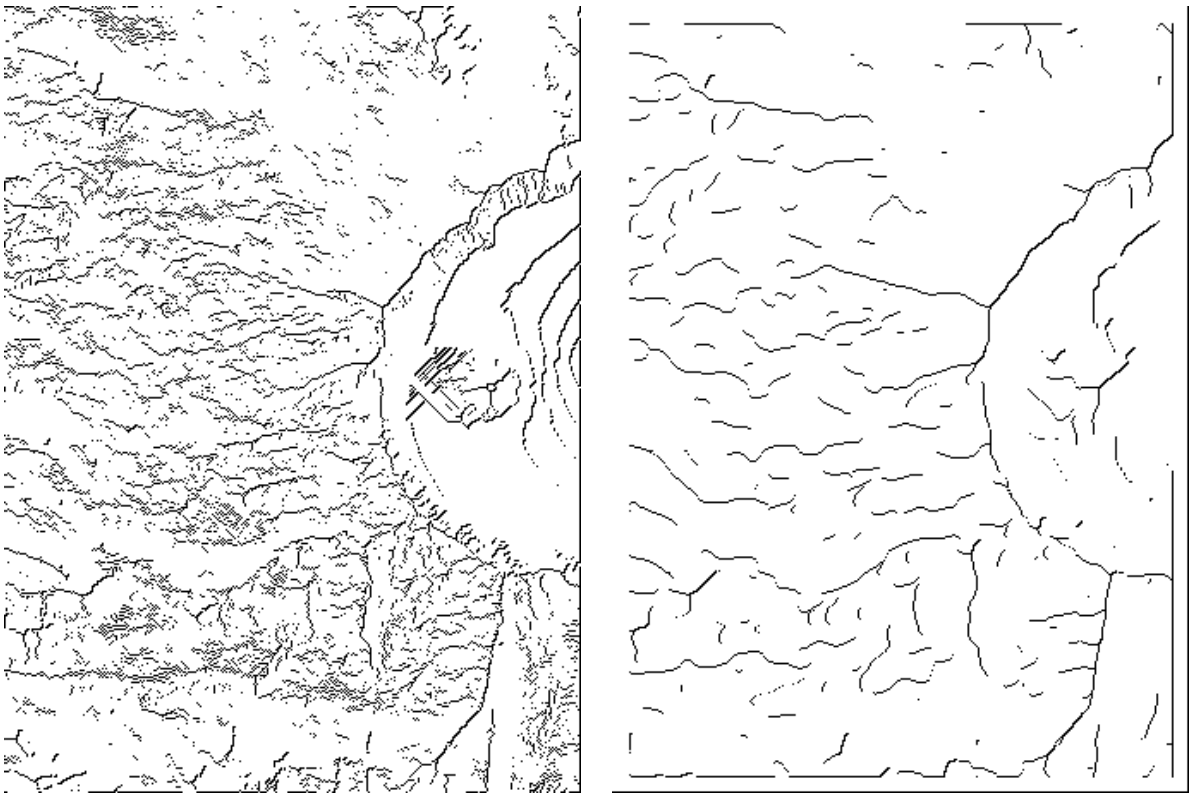

(a) (b)

Figure 4: The ridge lines found in the Crater Lake DEM by the marking method of Peucker and Douglas (a). In (b) the DEM has been smoothed by a Gaussian filter ($\sigma = 2.5$). Compare with Fig. 3(a).

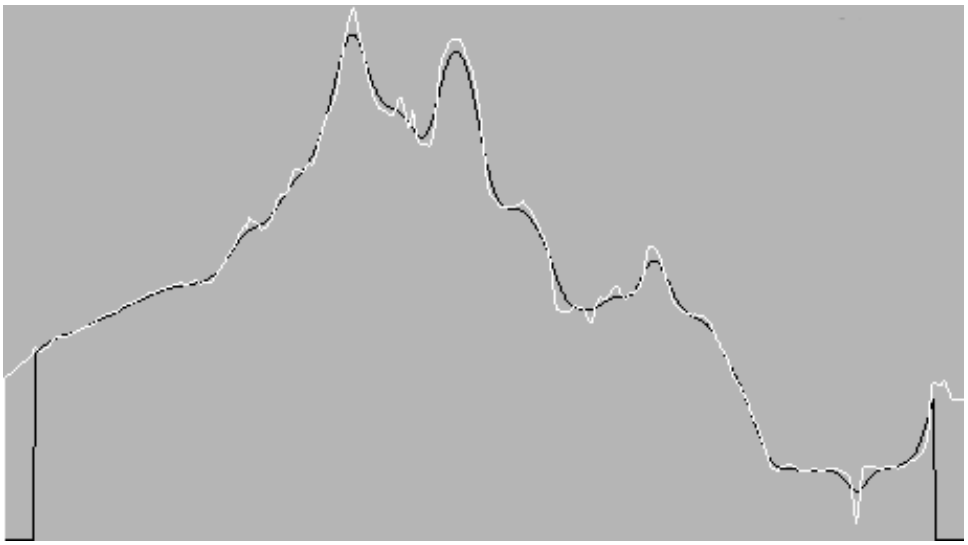

Figure 5: A slice along column 180 through Crater Lake (336 columns wide). White shows the original DEM; black the surface smoothed by Gaussian ($\sigma = 4.0$).

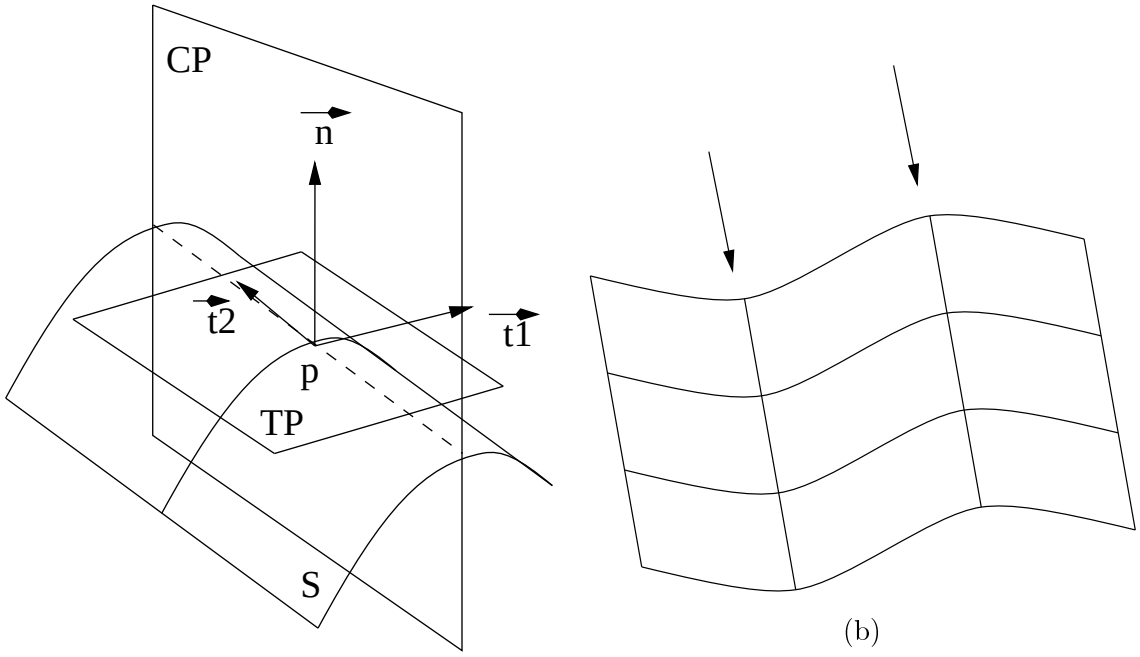


Figure 6: (a)Local surface geometry: the principal directions are orthogonal and $\vec{t_1}$ is the direction of maximum curvature. (b) Surface structural lines where curvature is locally maximal in direction $\vec{t_1}$.

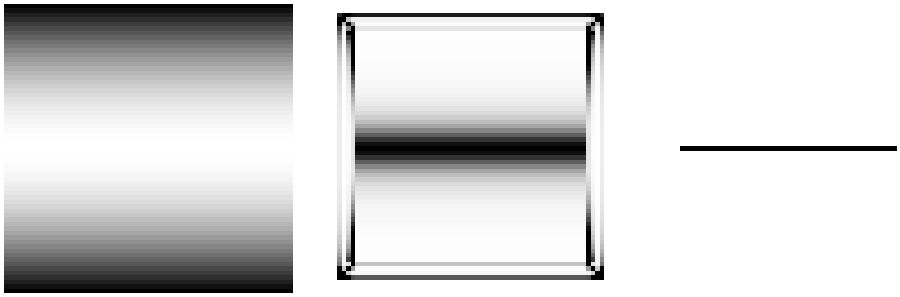

(a) (b) (c)

Figure 7: (a) Height image of the paraboloid; (b) Absolute value of maximum curvature $|k_1|$ for the paraboloid; (c) Locally maximal points in maximum curvature for the paraboloid

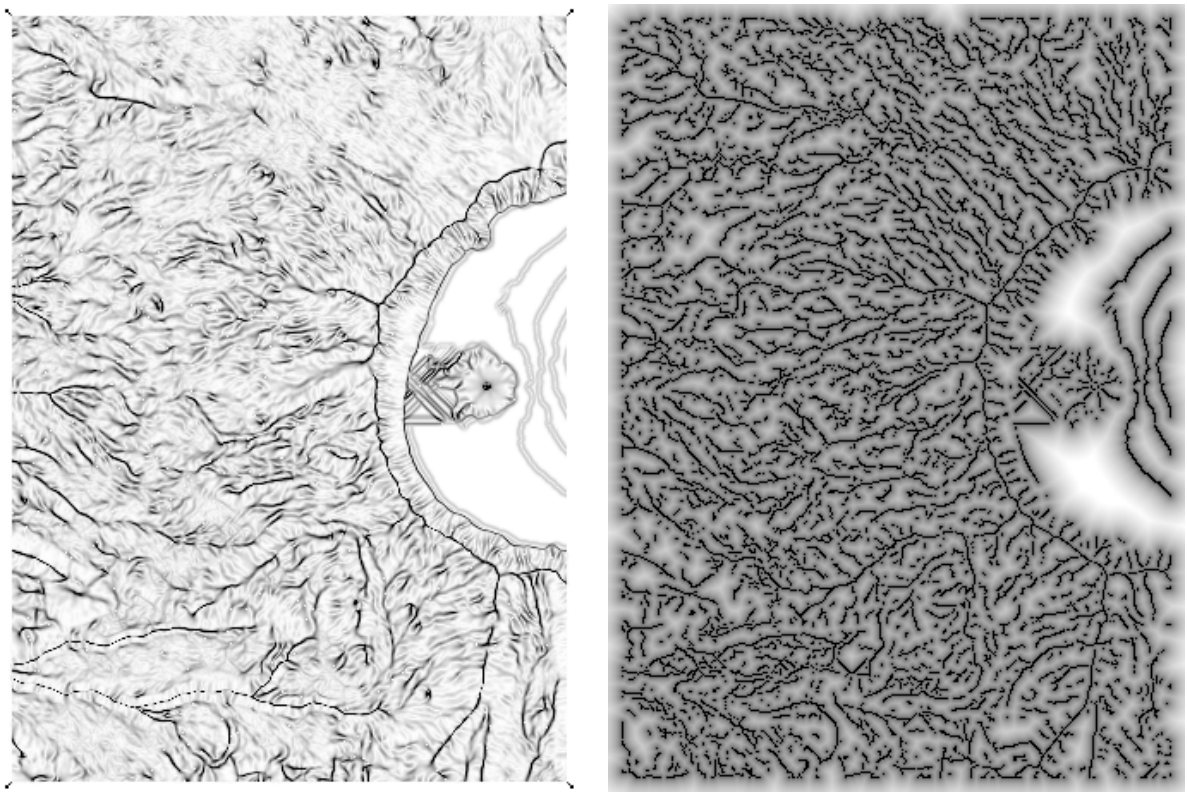

(a) (b)

Figure 8: (a) The absolute value of maximum curvature ($\sigma = 1.0$): darker is larger. (b) The proximity field for the fine scale ($\sigma = 1.0$) p-lines: brightness is proportional to distance from the line.

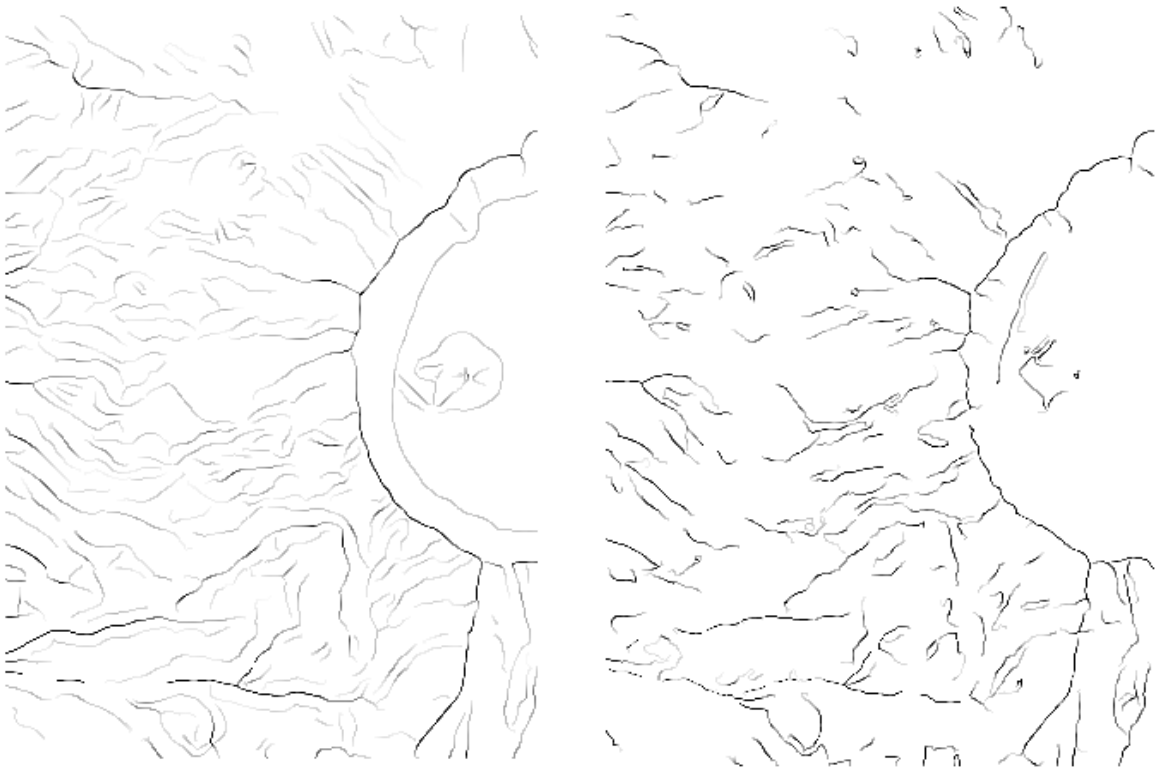

(a) (b)

Figure 9: (a) Local maximal curvature along the structural lines, at a medium scale. (b) Fine scale. These are the points found using non-maximum suppression.

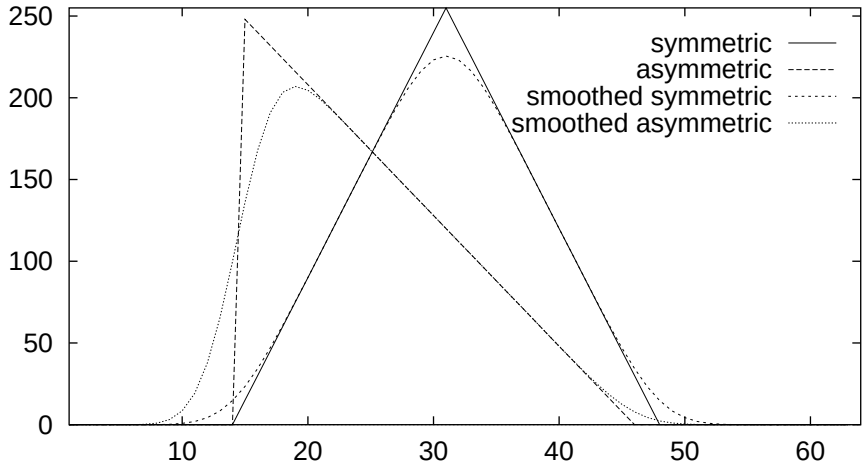


Figure 10: Smoothing an asymmetrical hill displaces the maximum, where the p-line lies, toward the shallower slope.

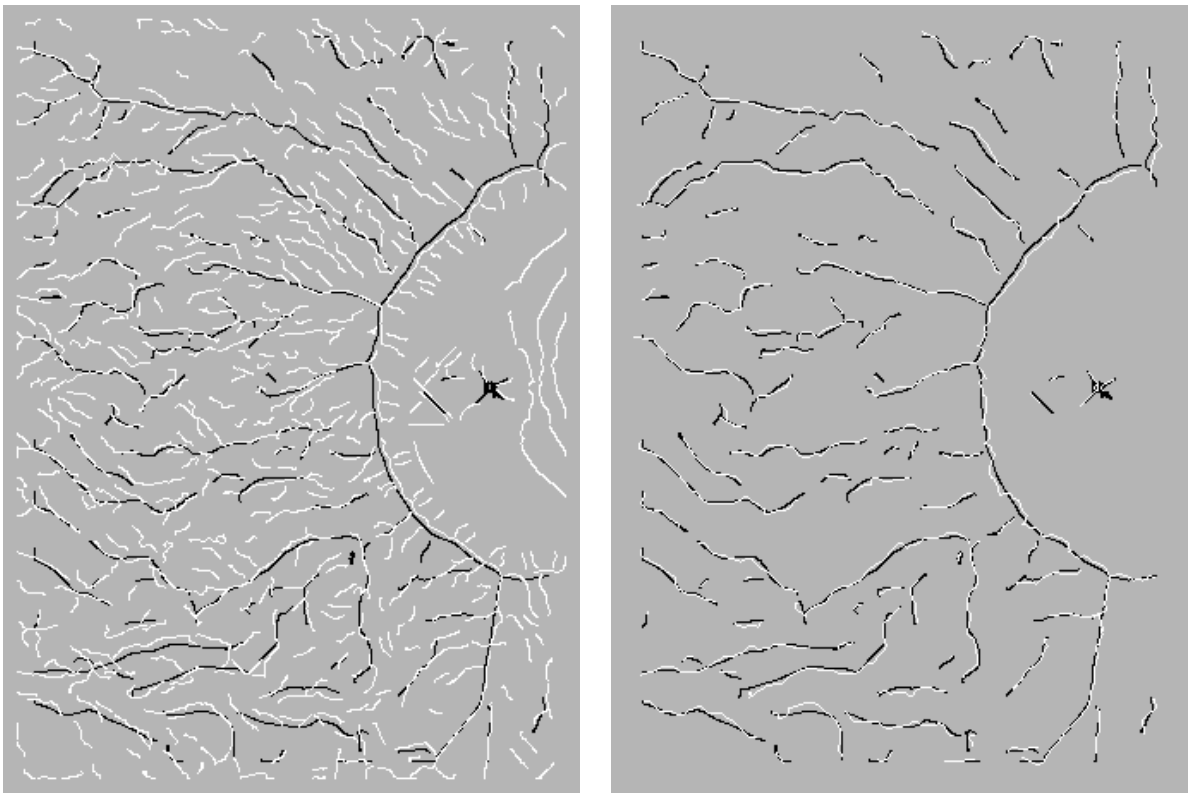

(a) (b)

Figure 11: (a) p-lines at fine scale ($\sigma = 1.0$) in white and p-lines at $\sigma = 4.0$ in black; (b) p-lines at $\sigma = 4.0$ in black with the corrected (snaked) result in white.

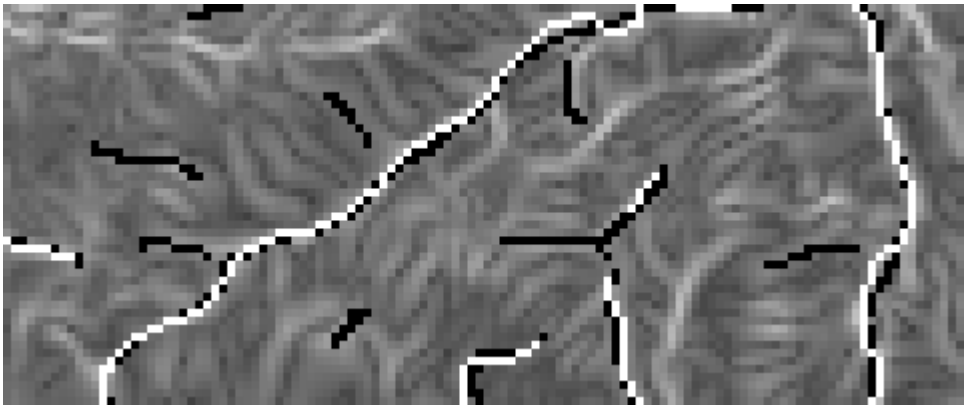

Figure 12: Snaking: $|k_1|$ appears in gray; brighter means higher values. Black shows the medium scale lines and white shows the snaked line. The black curve is pulled to brighter regions with higher attractive force.

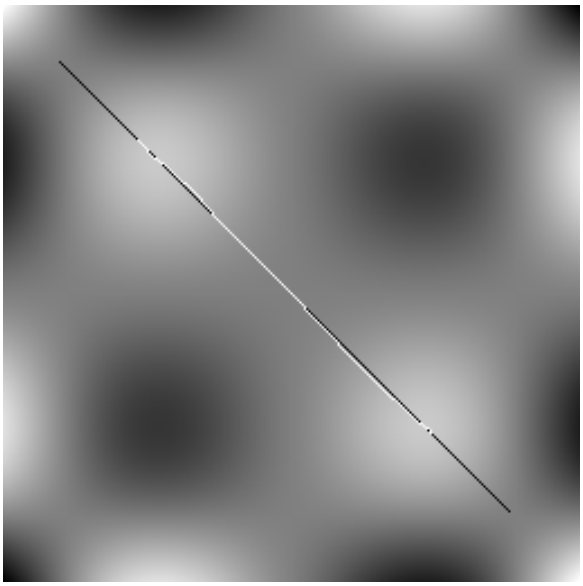

Figure 13: Retracting during snaking to a local maximum. The underlying maximum curvature field is shown in gray values, while the original curve is black and the result of snaking is white.

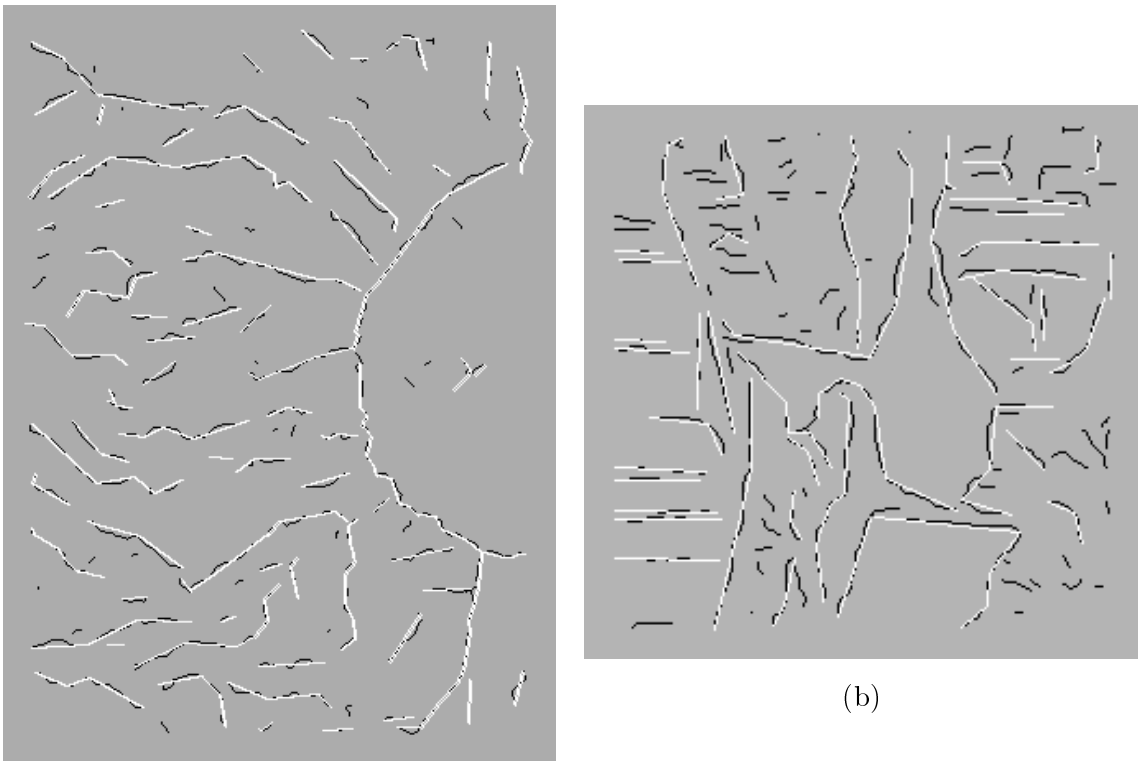

(a) (b)

Figure 14: (a) Snaked ($\sigma = 4.0$) p-lines in black and simplified lines, $gen = 20$, $minlength = 10$, result in white; (b) Snaked lines, both p- and n-, for Yakima in black and simplified lines, $gen = 15$, result in white.

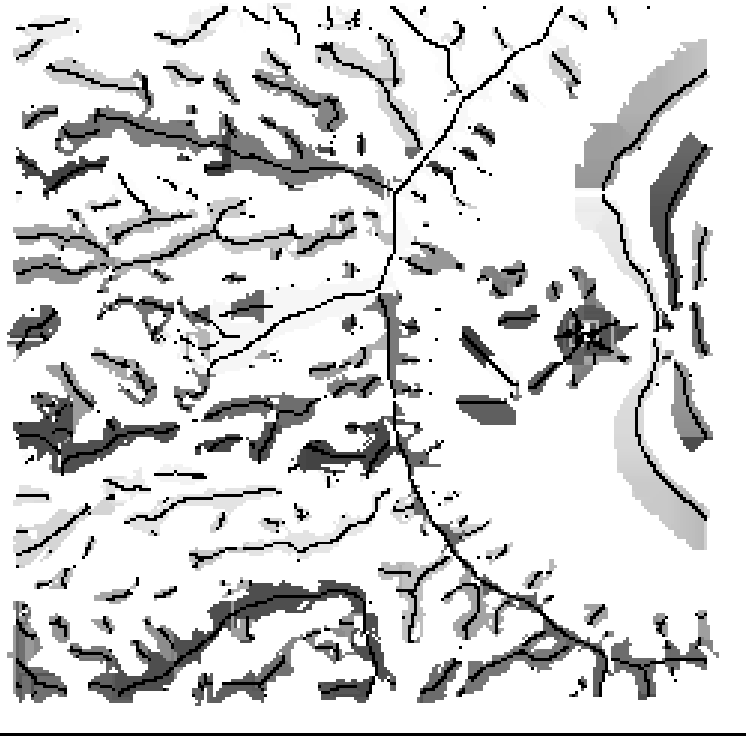

Figure 15: Regions of positive maximum curvature surrounding p-lines ($\sigma = 2.5$), for the central region of Crater Lake. The gray value of each region is the number of the p-line it surrounds. p-lines are shown in black.

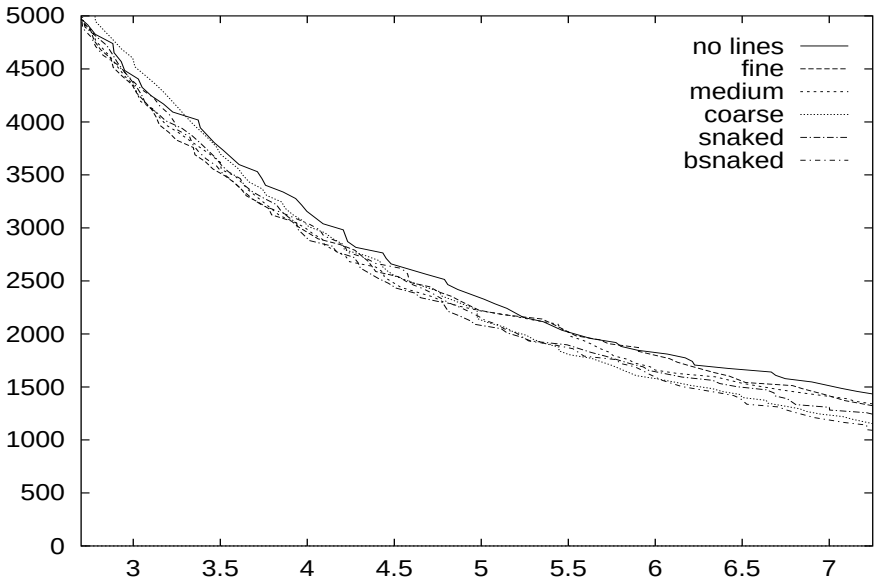


Figure 16: Number of points versus root-mean-square (RMSE) for Crater Lake.

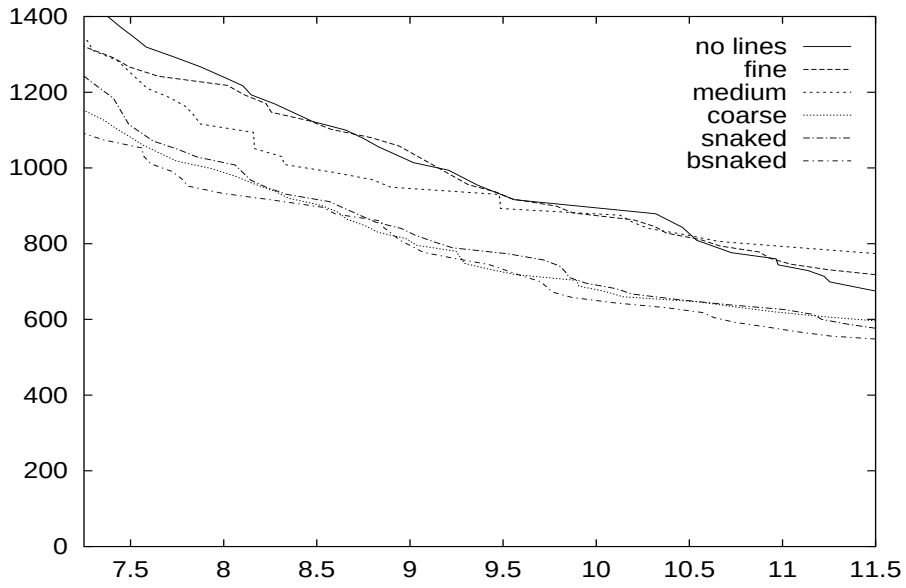


Figure 17: Number of points versus root-mean-square error (RMSE) for Crater Lake, rough approximations.

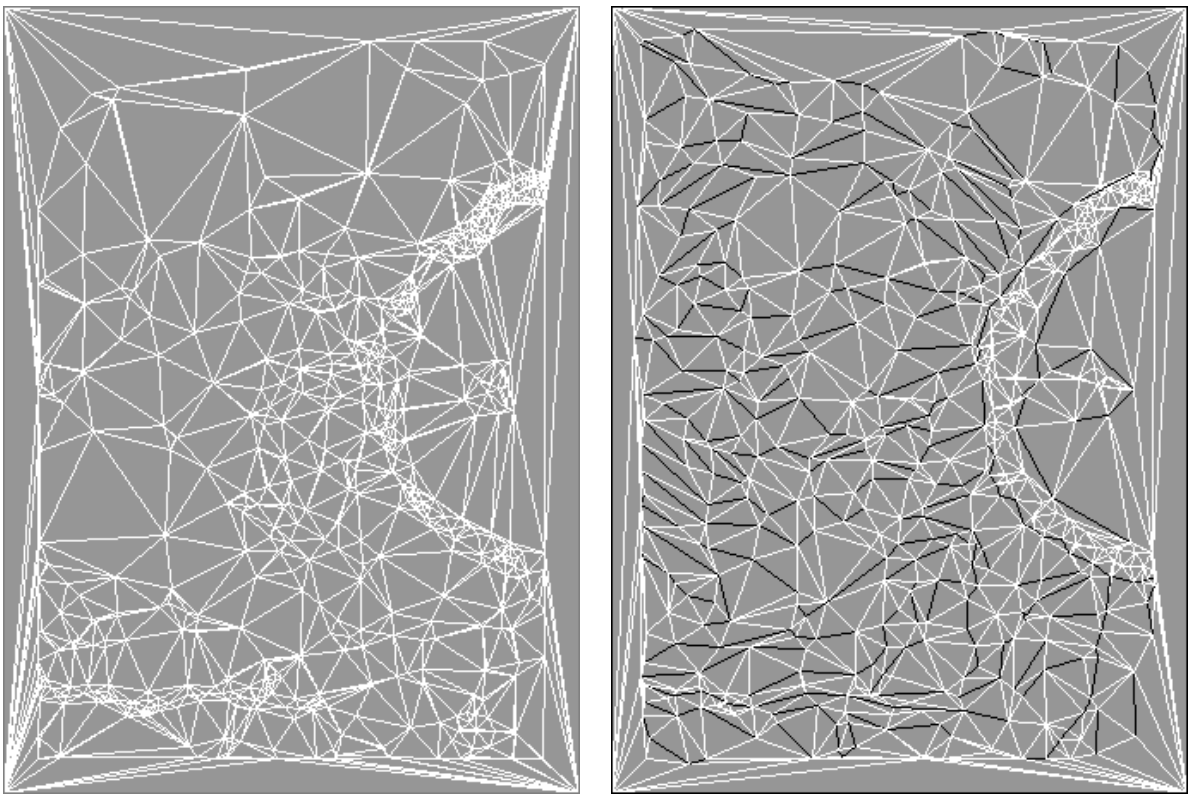

(a) (b)

Figure 18: (a) The triangulation (700 points) for no lines; (b) The triangulation (556 points) for csnaked–in both the constrained lines are shown in black and other edges in white.

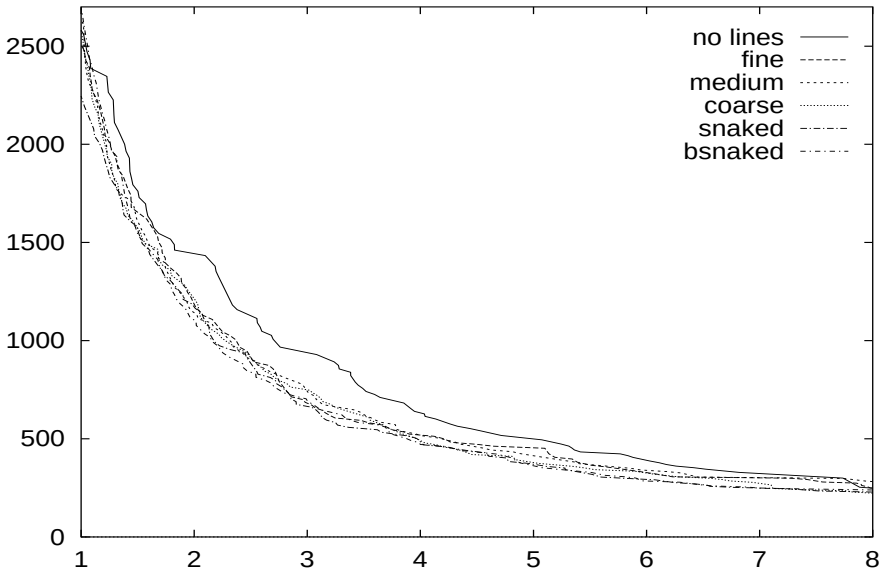


Figure 19: Number of points versus root-mean-square error (RMSE), for Yakima.

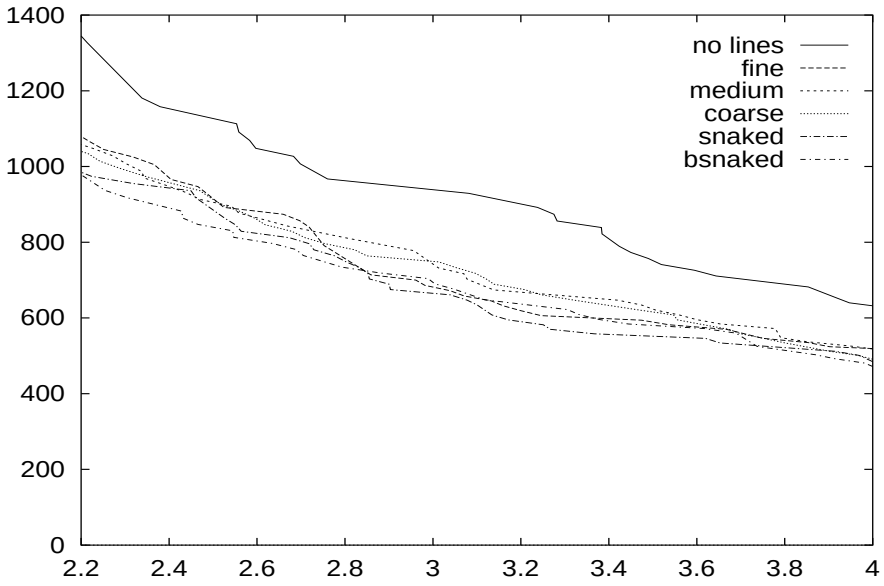


Figure 20: Number of points versus root-mean-square error (RMSE), rough approximations, for Yakima.

| | RMSE | | | MAE | | |
|---|---|---|---|---|---|---|
| range | 1.0-8.0 | 1.0-4.5 | 4.5-8.0 | 1.0-4.0 | 1.0-2.5 | 2.5-4.0 |
| fine | 0.866 | 0.834 | 0.896 | 0.675 | 0.700 | 0.654 |
| medium | 0.872 | 0.837 | 0.906 | 0.648 | 0.672 | 0.628 |
| coarse | 0.819 | 0.823 | 0.815 | 0.611 | 0.661 | 0.561 |
| snaked | 0.776 | 0.786 | 0.767 | 0.563 | 0.608 | 0.519 |
| csnaked | 0.788 | 0.798 | 0.778 | 0.584 | 0.627 | 0.542 |

Table 1: Average ratio of number of points for various structural lines, for RMSE, MAE and MAX, for several ranges in Yakima

| | RMSE | | | MAE | | | MAX | | |
|---|---|---|---|---|---|---|---|---|---|
| range | 2.8-11.8 | 2.8-7.3 | 7.3-11.8 | 2.1-8.1 | 2.1 -5.1 | 5.1-8.1 | 18-28 | 18-23 | 23 -28 |
| fine | 0.979 | 0.959 | 0.998 | 0.959 | 0.954 | 0.964 | 0.744 | 0.682 | 0.807 |
| medium | 0.963 | 0.946 | 0.980 | 0.920 | 0.938 | 0.902 | 0.738 | 0.690 | 0.786 |
| coarse | 0.863 | 0.921 | 0.804 | 0.801 | 0.894 | 0.705 | 0.691 | 0.656 | 0.725 |
| snaked | 0.869 | 0.920 | 0.818 | 0.829 | 0.908 | 0.749 | 0.682 | 0.692 | 0.672 |
| csnaked | 0.840 | 0.906 | 0.773 | 0.793 | 0.896 | 0.692 | 0.656 | 0.561 | 0.750 |

Table 2: Average ratio of number of points for various structural lines, for RMSE, MAE and MAX, for several ranges in Crater Lake.